MATLAB/Simulink-Based Simulation and Experimental Validation of a Novel Energy Storage System to a New Type of Linear Engine for Alternative Energy Vehicle Applications

Guizhou Ren

***Abstract*—This paper focuses on the research of simulation model and experiment of a novel energy storage system (ESS). This novel ESS is dedicated to supplying power flow effectively for a new type of linear engine, which is used in alternative energy vehicle firstly. The control strategy has been proposed based on the ESS model, which adopts bidirectional four modes of operation to control the power flow. To sufficiently discuss the ESS dynamic behavior, the performance of the novel ESS is analyzed using simulations based on MATLAB/Simulink and experiments based on digital signal processor TMS320F2812. Finally, simulation and experimental results have verified the effectiveness of the novel ESS and the accuracy of the control strategy.**

***Index Terms*—Alternative energy vehicle (AEV), dynamic model, energy storage system (ESS), linear engine, modeling, ultracapacitor (UC) banks.**

I. Introduction

THERE has been a growing global concern about the vehicle-generated greenhouse gas emissions, depleting fossil fuels, and the related air pollution in recent decades [1], [2]. Meanwhile, energy and environment have already become two crucial factors that limit the development of automotive industry [3]. In response, most of motor corporations focus their efforts on developing greener propulsion solutions for clean transportation in order to meet the ecological need and societal demand [4], [5]. Development of alternative energy vehicle (AEV) has been approved around the world. The AEV is different from the conventional vehicle and it takes advantage of the advanced technologies and the alternative and sustainable energy fuel [6]–[9]. Newly propulsion system is one of the keys toward AEV [10], [11]. Linear engine as a new type of vehicle propulsion system mainly used for AEVs such as hybrid electric vehicle, plug-in hybrid electric vehicle and extended-range electric vehicle, is under investigation by many research institutions worldwide [12]–[14]. A new type of linear engine is shown in Fig. 1, mainly including the combustion chamber for four-stroke internal combustion engine (ICE), linear electric generator (LEG), energy storage system (ESS), and control units [15]–[17].

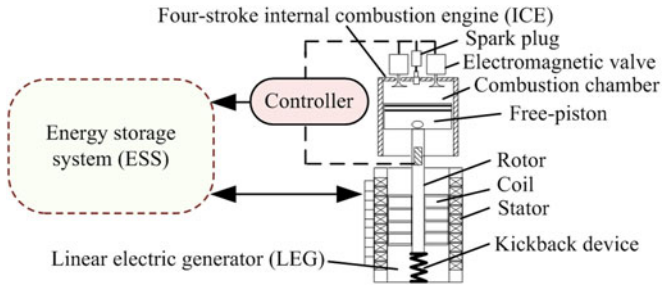

Fig. 1. Schematic diagram of a new type of linear engine.

A free-piston is connected with the rotor of LEG directly, and they as the moving parts do purely linear reciprocate movement together within the cylinder by operating LEG alternately as motor and generator periodically during four strokes, so chemical energy can be transformed into useful electrical energy that can be stored in ESS or used for load. The reciprocate movement is mainly determined by the instantaneous balance of the gas pressure in the combustion chamber, friction forces, the force of kickback device, and the electromagnetic force of LEG.

Applying Newton's second law of motion, equation of equilibrium of the moving masses is written as

$$m\frac{dv}{dt} = PS - (F_f + F_b + F_e) \tag{1}$$

where m is the mass of moving parts, v is the velocity of moving parts, P is the gas pressure in the combustionchamber, S is free-piston cross-sectional area, F_f is the total friction forces, F_b is the force of kickback device, F_e is the electromagnetic force of LEG.

The gas pressure in the combustion chamber is determined by the combustion process, friction forces are small during

Manuscript received April 5, 2016; revised July 24, 2017 and September 29, 2017; accepted December 5, 2017. Date of publication December 18, 2017; date of current version July 15, 2018. This work was supported in part by the National Natural Science Foundation of China under Grant 51407152, in part by the Open Fund of Fujian Key Laboratory of Automotive Electronics and Electric Drive (Fujian University of Technology) under Grant ZDKA17002, and in part by the Shandong Provincial Natural Science Foundation of China under Grant ZR2013EEL022. Recommended for publication by Associate Editor S. Williamson.

The author is with the Department of Vehicle Engineering, School of Electromechanical and Automotive Engineering, Yantai University, Yantai 264005, China (e-mail: renguizhou@tom.com).

Color versions of one or more of the figures in this paper are available online at http://ieeexplore.ieee.org.

Digital Object Identifier 10.1109/TPEL.2017.2784563

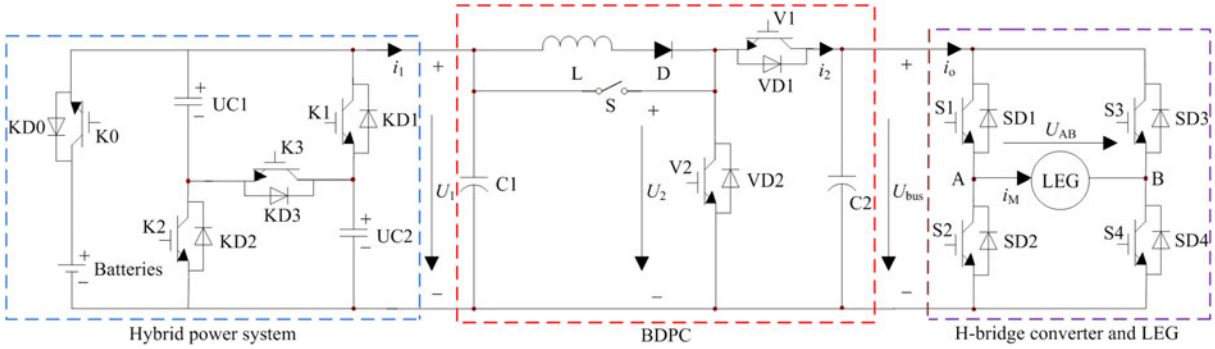

Fig. 2. Topology structure diagram of the novel ESS.

movement and can be ignored, the force of kickback device is determined by the helical compression spring. Therefore, the electromagnetic force of LEG should be controlled to realize the target motion of the free-piston.

The electromagnetic force of LEG can be obtained by

$$F_e = K_i i_M \tag{2}$$

where K_i is the electromagnetic force constant, i_M is the LEG current.

It is illustrated that the electromagnetic force developed by LEG is proportional to the armature current. The ESS supplies power to control the movement of the free-piston with the adjustable electromagnetic force when LEG is working in the motor operation (during the intake stroke and compression stroke). The power source is also used to cache the electric power output when LEG is working in the generator operation (during the power stroke and exhaust stroke).

In order to meet requirements, such as the regulation of electromagnetic force of LEG, the velocity of moving parts, bidirectional movement and high efficiency power flow of LEG, ESS needs to have the following characteristics: instantaneous charge/discharge capacity, control four-quadrant operation of LEG, achieve high-speed and accurate switching of LEG between motor state and generator state. A novel ESS for the new type of linear engine is presented, topology structure diagram of the novel ESS is shown in Fig. 2 [18], [19]. The novel ESS includes power source, nonisolated bidirectional power converter (BDPC) and H-bridge converter. In this system, the power source is alternately discharged (in the intake stroke and compression stroke) and charged (in the power stroke and exhaust stroke) in a very short period of time (about 80 ms). In addition, the power source needs to provide energy to electrical equipment of vehicle. So, the power source should have input-output instantaneous power response capability and have the ability to provide continuous and regulated energy to the in-vehicle electrical equipment. Therefore, the combination of ultracapacitor (UC) banks and battery banks is used as the hybrid power source, so the advantages of high power density of UC and high energy density of battery are fully utilized. UC banks are controlled by series-parallel switchover as power buffer to achieve energy release and absorption. The surplus energy will be diverted to battery banks which are connected in parallel with UC banks. This will assure that there will be no accumulation of energy in UC banks. Battery banks provide energy to the in-vehicle electrical equipment. It should be noted that the study of interconnection and control between UC banks and battery banks is a major and complex research topic. The detailed design of UC/battery hybrid power source will become the focus of our further research and is not presented in this paper.

As a novel system, the ESS used for four-stroke linear engine will have greater technical challenge and become a hotspot. Until recently there have been only a few published papers that primarily studied structure, working principle and extended application of the ESS [17]–[19]. However, there is a lack of systematic studies regarding detailed modeling approach and testing analysis of the above proposed ESS. This study is the first study which investigates modeling approach and experiment discussion of the proposed ESS for the four-stroke linear engine. The findings of this study mainly contribute to literature for a broader understanding of the novel ESS for the four-stroke linear engine application.

The aim of this paper is to provide simulation model and experiment studies of a novel ESS to linear engine for AEV applications, and the related techniques, such as mathematical model, simulation, and experiment have been presented and are discussed as follows. This paper is organized as follows. After the introduction section, dynamic models of the ESS are described in Section II. Simulation and experimental results are, respectively, given and discussed in Section III and IV. Conclusions are summarized in Section V.

II. System Description and Modeling

In this section, the details of the dynamic model of the novel ESS for linear engine are described. The system mainly consists of five parts: the UC banks which are switched over between series and parallel connections, the optimized BDPC which includes digital proportional integral derivative (PID) controller, the H-bridge converter which includes digital PID controller, the LEG of linear engine and the power flow control strategy. In order to verify the effectiveness of the proposed ESS [20]–[23], the MATLAB/Simulink and Simpower System software packages are selected as the modeling platform.

TABLE I
MAXWELL BOOSTCAP BCAP0650 UC CHARACTERISTICS

Parameters	Rated values
rated capacitance	650 [F]
energy density	3.29 [Wh/kg]
power density	5400 [W/kg]
capacitance tolerance	$+20\%/-5\%$ [−]
rated voltage	2.7 [V]
operating temperature range	$-40 \sim +65$ [°C]
ESR AC (1 kHz)	0.6 [mΩ]
ESR DC	0.8 [mΩ]
weight	0.20 [kg]
dimensions	$61.3(\phi) \times 79.5$ (H) [mm]

TABLE II
SPECIFICATIONS OF UC BANK

Parameters	Rated values
rated Voltage	62.1 [V]
number of cells	23 [–]
rated Capacitance	28 [F]
ESR DC	$\leq$40 [mΩ]
number of series	23 [–]
weight	$\leq$10 [kg]
volume	$<400 \times 200 \times 200$ [mm^3]

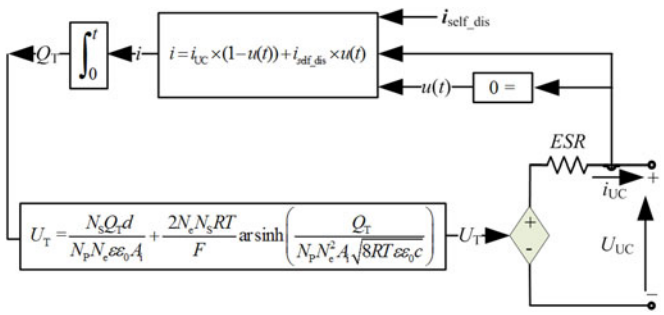

Fig. 3. Equivalent model for UC unit.

A. Dynamic Model of UC Banks With Series-Parallel Connections Switchover

The power source contains two identical UC banks. Each UC bank includes four parts: twenty-three 2.7-V BCAP0650 cells which are connected in series, cell balancing circuit, cooling devices, and sturdy packaging. The specifications of the UC cell and UC bank are given in Tables I and II, respectively.

Due to the hysteresis loop of the electrostatic energy storage method of UC is extremely thin, ranging from 85% to 98% [24], [25], the method has the advantage of higher energy efficiency during charging and discharging. So, the UC is selected for energy storage undergoing frequent charge and discharge cycles at high current and short duration. UC bank as a power buffer device can make full use of its advantage to output and assimilate power simultaneously. The equivalent circuit of UC unit is shown in Fig. 3 and the meanings of parameters of UC equivalent circuit are given in Table III [26].

In practical applications, multiple UCs can be combined in series to meet the required terminal voltage of UC storage system.

TABLE III
MEANINGS OF PARAMETERS OF UC EQUIVALENT CIRCUIT

Parameters	Meanings
A_i	interfacial area between electrodes and electrolyte
c	molar concentration
ESR	the charging and discharging resistance
F	the nominal capacitance
i_{UC}	charge/discharge current
U_{UC}	terminal voltage
Q_T	electric charge
d	molecular radius
T	operating temperature
ε	permittivity of material
ε_0	permittivity of free space
N_P	number of parallel UCs
N_S	number of series UCs

Meanwhile, in order to meet the demand of the total capacity, it is quite requested that a myriad of cells to be connected in parallel. The UC bank model has been implemented in MATLAB for this study.

This paper proposed a new solution which makes UC banks switched over between serial and parallel modes. The published papers on research of this technology are decidedly limited. A clear example of such a kind of solution can be found in [27], where a new power system based on series-parallel switchover of UC banks for pure electric vehicle (PEV) was proposed. The new power system mainly includes four UC banks and four semiconductor switches. The four UC banks can be changed over between series and parallel by controlling the four semiconductor switches. The results of actual running tests by a PEV show effectiveness and availability of this system. But, this kind of approach has significant drawbacks. First, during the system design, the UC banks are only used to absorb the regeneration energy during decelerations and release the stored energy during accelerations. Additionally, due to the difference of the operating voltage and capacitance of the four UC banks, the imbalance of power flow in UC banks may be occurred. Thus, we propose an efficient UC utilizing system, which uses series-parallel connections switchover for two UC banks. This solution is significantly different from the approach of [27]. By adopting this system, the four operating modes can be accomplished, and the balance of power flow in the two UC banks is controlled simultaneously. The UC banks switchover circuit can be seen from Fig. 2, and the changing over method will be described in the following section "power flow control strategy."

It is assumed that the rated voltage of each UC bank is U_C (see the circuit symbols marked in Fig. 2), the output voltage of UC banks is controlled by three switches, so the relationships of switch combinations and outputs are expressed as follows.

When UC banks are discharging

$$\begin{cases} U_1 = \begin{cases} U_C & K1 = K2 = K3 = 0 \\ 2U_C & K1 = K2 = 0, K3 = 1 \end{cases} \\ i_1 = \frac{U_{\mathrm{bus}} \times i_o}{U_1} \end{cases} \tag{3}$$

TABLE IV
RELATIONSHIPS OF UC BANKS AND SWITCHES

States of charge/discharge	States of series/parallel	States of switches		
		$K1$	$K2$	$K3$
discharge	parallel	0	0	0
discharge	series	0	0	1
charge	parallel	1	1	0
charge	series	0	0	0

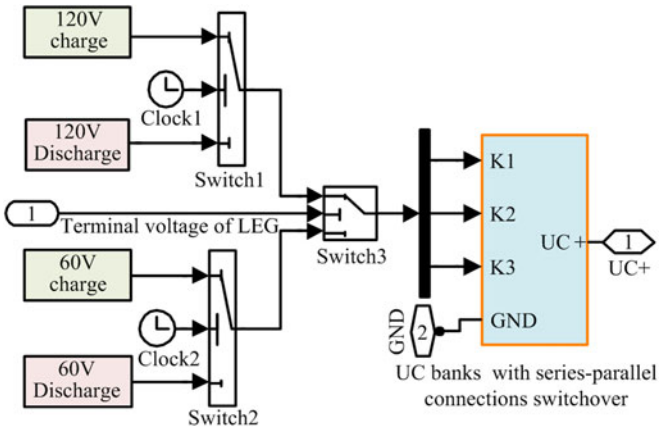

Fig. 4. Simulink model for controlling UC banks switchover between serial and parallel in charge/discharge mode.

where U_1 is the output voltage of UC banks, i_1 is the current of UC banks, i_o is the output current of BDPC, $U_{\rm bus}$ is the output voltage of BDPC (it also is the bus voltage). $K1, K2$ and $K3$ are the logical variables of switches (K1, K2, and K3), respectively. The state "1" refers to turn ON, while the state "0" refers to turn OFF, the same as the following descriptions.

When UC banks are charging

$$\begin{cases} U_1 = \begin{cases} U_C & K1 = K2 = 1, K3 = 0 \\ 2U_C & K1 = K2 = K3 = 0 \end{cases} \\ (-i_1) = \frac{U_{\rm bus} \times (-i_o)}{U_1} \end{cases}. \tag{4}$$

The relationships of UC banks and switches are given in Table IV.

Simulink model for controlling UC banks switchover between serial and parallel in charge/discharge mode is shown in Fig. 4. In this simulink model, the terminal voltage of LEG as the control input (the second input) is accepted by the switch3 block, and the switch3 block threshold is set to 120 V (the voltage of two series connected UC banks). If the control input is greater than or equal to the threshold value, the first input is passed, otherwise, the third input is passed. The first input of the switch3 block is "120 V charge mode" or "120 V discharge mode," the third input of the switch3 block is "60 V charge mode" or "60 V discharge mode," and 60 V is the voltage of two parallel connected UC banks. Each of the four modes (120 V charge mode, 120 V discharge mode, 60 V charge mode, and 60 V discharge mode) represents the states of three switches (as described in Table IV). In addition, the switch1 and switch2 block threshold values are set to 37.5 ms (the alternating moment of charge mode and discharge mode). Output voltage of UC banks is obtained by controlling the switches (K1, K2, and K3), so series-parallel connections switchover for UC banks is achieved. The model of the UC banks that are switched over between serial and parallel is shown in Fig. 5.

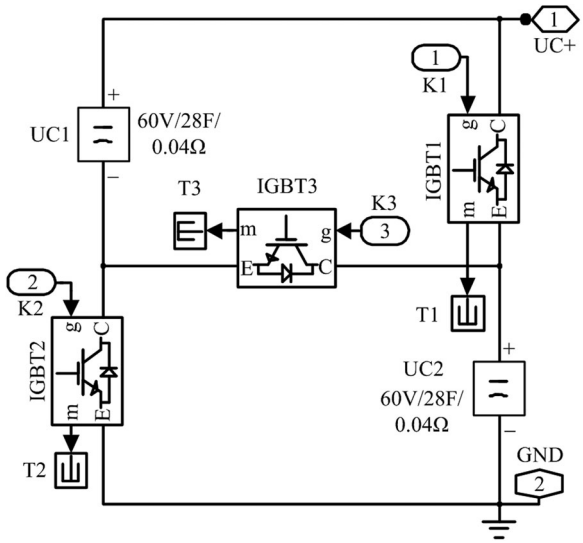

Fig. 5. Model of the UC banks that are switched over between serial and parallel.

B. Dynamic Model of BDPC

In this system, a nonisolated BDPC is used to connect UC banks with LEG (there is H-bridge converter between BDPC and LEG). The BDPC is required to operate in both the buck and boost modes with bidirectional power control. It is also possible to control power flow between UC banks and LEG in either directions.

For sizing the inductor of BDPC, the important parameters are the peak inductor current and inductance since they determine the inductor energy-handling requirement. Cost and size of the inductor are related to energy stored in the inductor.

A single inductor in BDPC acts as a boost inductor in step-up mode and also as a filter inductor in step-down mode, the following equations size the inductor of BDPC

$$L_{\rm min} = \max(L_{\rm boost}, L_{\rm buck}) \tag{5}$$

$$I_{\rm LP} = \max(I_{\rm boost\_LP}, I_{\rm buck\_LP}) \tag{6}$$

where $L_{\rm boost}$ and $I_{\rm boost\_LP}$ are, respectively, the inductance and the peak current of inductor for boost operation, $L_{\rm buck}$ and $I_{\rm buck\_LP}$ are, respectively, the inductance and the peak current of inductor for buck operation.

It is important note that the ESS has the feature of unbalanced power flow in both directions. During the boost mode (i.e., UC banks being discharged), it is considered that the BDPC is operated at the maximum output power of 9.6 kW and output voltage of 240 V, so the output current becomes 40 A. During the buck mode (i.e., UC banks being charged), it is considered that the BDPC is operated at the maximum input power of

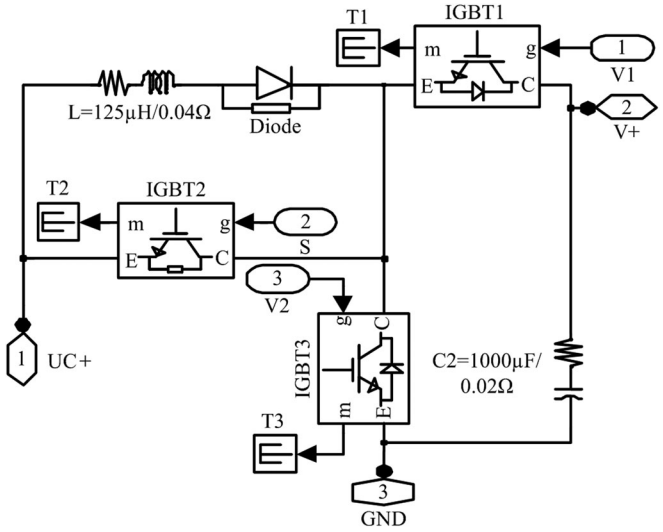

Fig. 6. BDPC model.

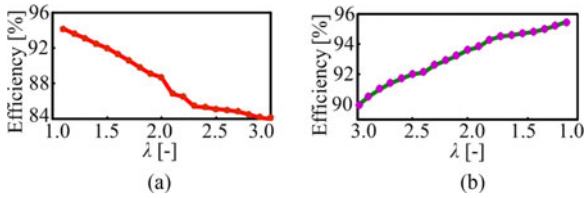

Fig. 7. $\eta - \lambda$ characteristics of conventional BDPC by experiment. (a) Operation in the boost mode. (b) Operation in the buck mode.

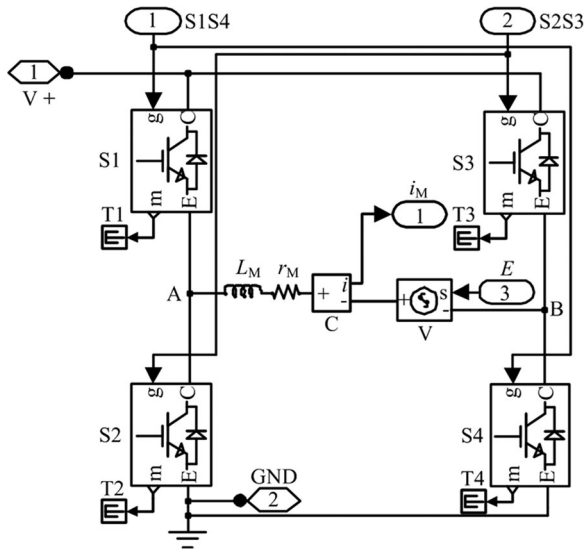

Fig. 8. H-bridge converter with LEG model.

30 kW and input voltage of 300 V, so the input current becomes 100 A. According to the design specifications of the BDPC and the inductor design rule, boost operation (i.e., power flow from UC banks to LEG) is for the peak inductor current $I_{\mathrm{boost\_LP}} = 88$ A and inductance $L_{\min} = 125\,\mu$H (energy-handling requirement 0.484 J) under the maximum power condition (about 9.6 kW), and buck operation (i.e., power flow from LEG to UC banks) is for the peak inductor current $I_{\mathrm{buck\_LP}} = 300$ A and inductance $L_{\min} = 69.4\,\mu$H (energy-handling requirement 3.123 J) under the maximum power condition (about 30 kW). Thus, the desired inductance $L_{\min} = 125\,\mu$H and the peak current $I_{\mathrm{LP}} = 300$ A of inductor are obtained by implementing the design equations of (5) and (6), and the stored energy in inductor is 5.625 J.

It is clear that the peak current of inductor is larger for BDPC operating on the buck mode (power flow from LEG to UC banks) than that for BDPC operating on the boost mode (power flow from UC banks to LEG), this leads to a very heavy and bulky inductor. Furthermore, the UC banks as power buffer can directly receive the pulse-width modulation (PWM) signal and may not need the filter inductor to smooth waveform. Therefore, an optimized topology of BDPC used in the novel ESS is designed [28]. Main feature of the optimized design topology is to bypass the filter inductor (L) by controlling power switch (S) when UC banks are charged in buck mode, the inductor in BDPC is only used as a boost inductor in boost mode, so the desired inductance $L_{\min} = 125\,\mu$H and the peak current $I_{\mathrm{LP}} = 88$ A of inductor are needed, and the stored energy in inductor is 0.484 J. This design can effectually reduce the volume and cost of the inductor. It is well positioned to meet the requirements of ESS. In [28], the characteristics of the proposed BDPC have been verified by experiments. The BDPC model is shown in Fig. 6, and the application of the BDPC also will be described in the following section "power flow control strategy."

It is a critical issue to improve the conversion efficiency of BDPC over a wide range of input and output voltages, which will directly affects the overall efficiency of ESS. The voltage conversion ratio of BDPC should be not too high [29], [30], where η is defined as the efficiency of BDPC and λ is defined as the voltage conversion ratio of BDPC. The $\eta - \lambda$ characteristics of conventional BDPC obtained by experiment are illustrated in Fig. 7. It is clear to note that the voltage conversion ratio should be as small as possible under wide voltage range in order to achieve excellent efficiency. In this system, the voltage conversion ratio of BDPC is always controlled within the ideal range (2 to 3) under wide voltage range due to the use of the series-parallel connections switchover technology for UC banks [31].

C. Dynamic Model of H-Bridge Converter and LEG

The polarity of generated back EMF when LEG working in generator mode is at every moment opposite to UC banks terminal voltage. An H-bridge converter between BDPC and LEG is built with four insulated gate bipolar transistor (IGBT) switches and free-wheeling diodes, which is used to reverse the polarity of the back EMF and can also be used to provide a path for current from LEG to power source when all four of IGBTs are turned OFF. So, the power flow in four quadrants can be achieved. The H-bridge converter with LEG model is shown in Fig. 8. Assuming that the duty cycle of S1 and S4 is D_H, then, the duty cycle of S2 and S3 is $(1 - D_H)$, the switching period is T. Fig. 8 also shows the equivalent circuit of LEG. The model consists of an inductance L_M, an equivalent resistance r_M, the back EMF E, and the armature current i_M.

The state mathematical models of H-bridge converter and LEG are as follows.

State I $(0 < t \leq D_H T)$*:* S1 and S4 on, the terminal voltage of LEG $U_{\rm AB}$ can be stated as

$$\begin{cases} U_{\rm AB} = L_M \frac{di_M}{dt} + r_M \times i_M + E \\ U_{\rm AB} = U_{\rm bus}. \end{cases} \tag{7}$$

where $U_{\rm bus}$ is the bus voltage.

State II $(D_H T < t \leq T)$*:* S2 and S3 on, the terminal voltage of LEG $U_{\rm AB}$ can be expressed by

$$\begin{cases} U_{\rm AB} = L_M \frac{di_M}{dt} + r_M \times i_M + E. \\ U_{\rm AB} = -U_{\rm bus} \end{cases} \tag{8}$$

In state I, we assume that the initial current of LEG is i_{M0}, the on-time of S1 and S4 is $t_{\rm on}$, then, the armature current is given by

$$i_{1M}(t) = i_{M0} e^{-t/\tau} + (1 - e^{-t/\tau}) \frac{U_{\rm bus} - E}{r_M} \tag{9}$$

where, $\tau = L_M / r_M$ is the time constant.

In state II, the off-time of S1 and S4 is $(t - t_{\rm on})$, we assume that the initial current of LEG is i_{M1}, then, the armature current is given by

$$i_{2M}(t) = i_{M1} e^{-(t-t_{\rm on})/\tau} - (1 - e^{-(t-t_{\rm on})/\tau}) \frac{U_{\rm bus} + E}{r_M}. \tag{10}$$

So, the average terminal voltage of LEG $\bar{U}_{\rm AB}$ during one switching period can be expressed as

$$\begin{aligned} \overline{U}_{\rm AB} &= \frac{D_H T \times U_{\rm bus} + (1 - D_H) \times (-U_{\rm bus})}{T} \\ &= (2D_H - 1) U_{\rm bus}. \end{aligned} \tag{11}$$

D. Power Flow Control Strategy

In order to ensure stable, reliable and efficient operations for the system, a proper power flow control strategy is needed to make ESS have high accuracy in the steady state and fast response capability in the transient state [32]. Bidirectional four operating modes are implemented. The four operating modes are as follows: step-down in motor status, step-up in motor status, step-down in generator status, and step-up in generator status. Meanwhile, in order to illustrate the stability of the controller, we made test with the ESS by suddenly connecting the linear engine at the output of the LEG.

1) Mode I: Step-Down in Motor Operation: In this mode, LEG works as an electric motor and is powered by the UC banks. When the required voltage of LEG $(U_{\rm AB})$ is below the terminal voltage of two parallel-connected UC banks $(U_{\rm C})$, K1, K2, and K3 are turned OFF so that UC1 and UC2 are discharged in parallel (60 V-discharge-mode). H-bridge converter is controlled to regulate the terminal voltage of two parallel-connected UC banks down to the desired voltage of LEG.

V1 and V2 are turned OFF, S is turned ON. The four IGBTs of H-bridge converter are controlled by PWM signals, so the required voltage of LEG is achieved by adjusting the duty cycle of the signal which drives one leg of the H-bridge converter, D_H. Fig. 9 shows step response of the armature current of LEG, it should be noted that $i_{M\,\rm ref}$ is the reference armature current which is proportional to the required electromagnetic force of LEG. It can be seen that the armature current of LEG reaches the reference value quickly and without any overshoot, and the current tracking error under steady state is nearly zero. Also, the required terminal voltage of LEG is shown in Fig. 9.

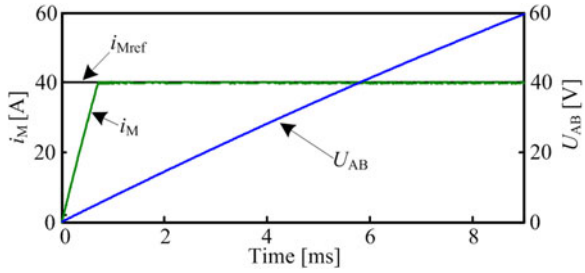

Fig. 9. Armature current step response and the terminal voltage of LEG in step-down operating mode I.

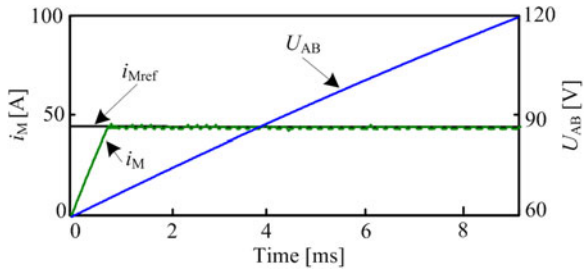

Fig. 10. Armature current step response and the terminal voltage of LEG in step-up operating mode II.

2) Mode II: Step-Up in Motor Operation: In this mode, LEG also works as an electric motor and is powered by the UC banks. When the required voltage of LEG $(U_{\rm AB})$ exceeds the terminal voltage of two parallel-connected UC banks (U_C) and is below the terminal voltage of two series-connected UC banks $(2U_C)$, K1, K2, and K3 are turned OFF so that UC1 and UC2 are discharged in parallel (60 V-discharge-mode). When the required voltage of LEG $(U_{\rm AB})$ exceeds the terminal voltage of two series-connected UC banks $(2U_C)$, K1 and K2 are turned OFF, K3 is turned ON, so that UC1 and UC2 are discharged in series (120 V-discharge-mode). BDPC is controlled to regulate the terminal voltage of two parallel-connected UC banks up to the desired voltage of LEG.

V1 is turned OFF, V2 is controlled by PWM signal, BDPC acts as a boost converter and the power flows from UC banks to LEG. The four IGBTs of H-bridge converter are controlled by PWM signals, so the required armature current of LEG is obtained by adjusting the duty cycle of the signal which drives one leg of the H-bridge converter, D_H. Fig. 10 shows step response of the armature current of LEG, it can be seen that the armature current of LEG reaches the reference value quickly and without any overshoot, and the current tracking error under steady state is nearly zero. Also, the required terminal voltage of LEG is shown in Fig. 10.

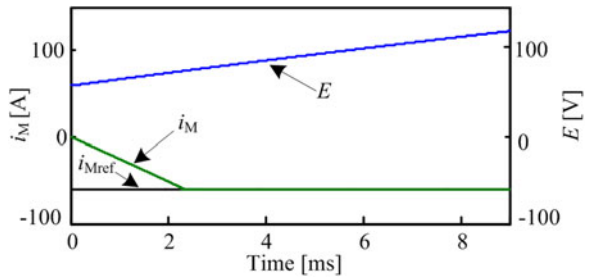

Fig. 11. Armature current step response and the terminal voltage of LEG in step-down operating mode III.

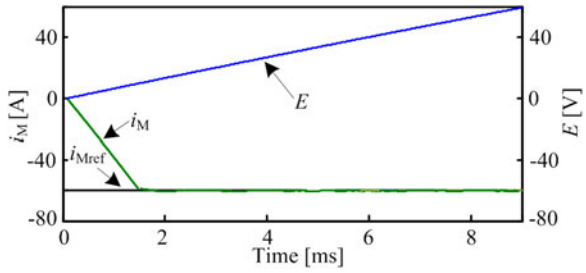

Fig. 12. Armature current step response and the terminal voltage of LEG in step-up operating mode IV.

In the above two operating modes, UC1 and UC2 are simultaneously discharged, which means that the power flow between the two UC banks is evenly distributed. So, a stable discharge balance can be achieved between UC1 and UC2.

3) Mode III: Step-Down in Generator Operation: In this mode, LEG acts as a generator to charge the UC banks via the BDPC. When the back EMF of LEG (E) exceeds the terminal voltage of two series-connected UC banks ($2U_C$), K1, K2, and K3 are turned OFF so that UC1 and UC2 are charged in series (120 V-charge-mode). When the back EMF of LEG (E) exceeds the terminal voltage of two parallel-connected UC banks (U_C) and is below the terminal voltage of two series-connected UC banks ($2U_C$), K1 and K2 are turned ON, K3 is turned OFF so that UC1 and UC2 are charged in parallel (60 V-charge-mode). The BDPC is controlled to regulate the back EMF of LEG down to the terminal voltage of two UC banks.

V1 is controlled by PWM signal, V2 is turned OFF, S is turned ON. BDPC acts as a buck converter and the power flows from LEG to UC banks. The four IGBTs of H-bridge converter are controlled by PWM signals, so LEG's movement is controlled by adjusting the duty cycle of the signal which drives one leg of the H-bridge converter, D_H. Fig. 11 shows step response of the armature current of LEG, it can be seen that the armature current of LEG reaches the reference value quickly and without any overshoot, and the current tracking error under steady state is nearly zero. Also, the terminal voltage of LEG is shown in Fig. 11.

4) Mode IV: Step-Up in Generator Operation: In this mode, LEG also acts as a generator to charge the UC banks via the BDPC. When the back EMF of LEG (E) is below the terminal voltage of two parallel-connected UC banks (U_C), K1 and K2 are turned ON, K3 is turned OFF so that UC1 and UC2 are charged in parallel (60 V-charge-mode). The BDPC is controlled to regulate the back EMF of LEG up to the terminal voltage of two parallel-connected UC banks.

V1 and S are turned ON, V2 is turned OFF. The four IGBTs of H-bridge converter are controlled by PWM signals, so the step-up operation is implemented by using the inductance of LEG and adjusting the duty cycle of the signal which drives one leg of the H-bridge converter, D_H. Fig. 12 shows step response of the armature current of LEG, it can be seen that the armature current of LEG reaches the reference value quickly and without any overshoot, and the current tracking error under steady state is nearly zero. Also, the terminal voltage of LEG is shown in Fig. 12.

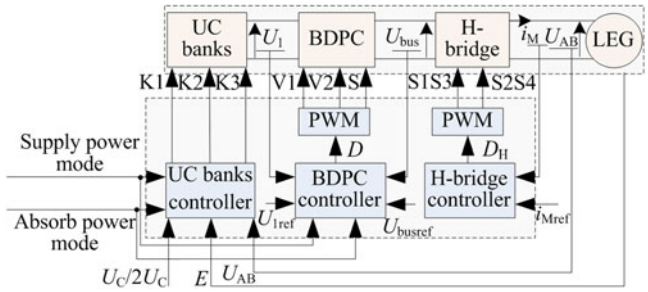

Fig. 13. Control system of ESS.

In the above two operating modes, UC1 and UC2 are simultaneously charged, which means that the power flow between the two UC banks is evenly distributed. So, a stable charge balance can be achieved between UC1 and UC2.

It should be noted that we have applied the PID control scheme for the armature current regulation in four operating modes, the results show that the PID controller has significantly faster transient response and steady-state response.

E. Controller

All of the operations outlined in the previous section must be controlled by a microprocessor which discriminates the working condition and makes the appropriate decisions for each particular situation. The TMS320F2812 fixed-point 32-bit digital signal processor (DSP) from Texas Instruments is used in order to implement the control system. The main parameters (such as U_1, i_1, U_{AB}, i_M and $U_{\rm bus}$) are obtained from specially installed sensors, and all of these parameters are acquired by the analog/digital (A/D) converter module contained in DSP. DSP is also responsible for system protection actions, i.e., over voltage, over current, and over temperature. The control system of ESS is shown in Fig. 13, it mainly consists of UC banks controller, BDPC controller and H-bridge converter controller.

The required voltage of LEG in motor operation and back EMF of LEG in generator operation are received by UC banks controller and compared, respectively, with the set voltages. Output voltage of UC banks is calculated according to the operation mode and obtained by controlling the switches (K1, K2, and K3), so series-parallel connections switchover for UC banks is achieved. Flag signals of the motor operation and generator operation are received by BDPC controller. The control

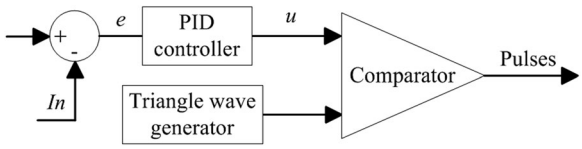

Fig. 14. Control of PWM signal generation.

objectives are bus voltage $(U_{\rm bus})$ in motor operation and terminal voltage (U_1) in generator operation. Duty cycle is calculated according to the operation modes and the requirements of power flow, the switches (V1, V2, and S) of BDPC are controlled by PWM signals, which are generated by the controller in accordance with the corresponding duty cycle. The control of PWM signal generation is shown in Fig. 14.

The armature current of LEG is received by H-bridge converter controller and compared with the required current. The switches (S1, S2, S3, and S4) of H-bridge converter are controlled by PWM signals, which are generated by the controller in accordance with the corresponding duty cycle. The BDPC and H-bridge converter are controlled by digital PID controllers to regulate bus voltage and LEG current.

In order to obtain a reliable, stable, and efficient operation for the control system, the designed digital PID controllers need to have the following advantages: excellent stability and robustness even for load variations, superior dynamic response, and simple implementation. Thus, the incremental PID control algorithm is applied in the control system to realize the bus voltage of controlled incline to the set value, so the adaptability and stability of the system are enhanced. Regarding the transitions dramatic properties of the LEG current, differential forward PID control algorithm is adopted in LEG current controlling to avoid swells or sags caused when the system oscillation, so the dynamic performance of the system is significantly improved. Differential forward PID control algorithm can be expressed as

$$\begin{cases} u(k) = k_p e(k) + k_i \sum_{j=0}^{k} e_j \\ y(k) = c_1 y(k-1) + c_2 u(k) - c_3 u(k-1) \end{cases} \tag{12}$$

where k_p is the proportional coefficient, k_i is the integral coefficient, $e(k)$ is the error between the reference and plant output, and is the input of the controller, $u(k)$ is the control variable and is the output of the controller, $y(k)$ is the actual output of the system. We assume that T_c is the sampling period, γ is constant, and $\gamma < 1, c_1, c_2$, and c_3 can be got by $c_1 = (k_d/k_p)/(k_d/k_p + T_c), c_2 = (\gamma k_d/k_p + T_c)/(k_d/k_p + T_c), c_3 = (\gamma k_d/k_p)/(k_d/k_p + T_c), k_d$ is the differential coefficient.

The digital PID controllers are shown in Fig. 15.

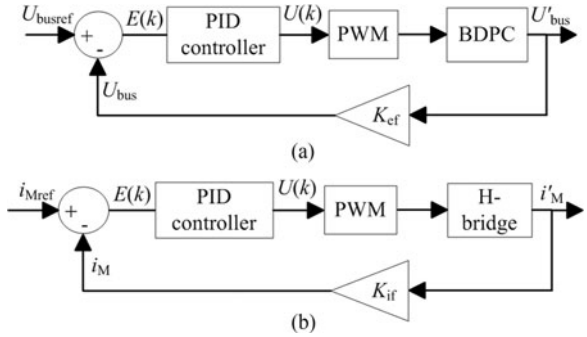

Fig. 15. Digital PID controllers. (a) Block diagram of the bus voltage control. (b) Block diagram of the LEG current control.

III. Simulation Results and Discussion

The mathematical model of the system described above is simulated in MATLAB's Simulink environment. Fig. 16 shows the simulation blocks. It consists of four principal subsystems: UC banks, H-bridge converter and LEG, BDPC, and controllers. Each of the subsystems contains different blocks to represent associated mathematical models. The specification of LEG is shown in Table V and simulation parameters of LEG are given in Table VI.

The tracking of armature current is illustrated in Fig. 17. It is the intake stroke from 0 to 17.5 ms. In the time interval from 0 to 10 ms, the armature current is set to be 45 A in order to obtain stable electromagnetic force, and LEG is doing acceleration movement [from top dead center of stroke (TDC) to bottom dead center of stroke (BDC)]. In the time interval from 10 to 17.5 ms, the electromagnetic force is not required, so the armature current is set to be of zero.

It is the compression stroke from 17.5 to 37.5 ms. LEG is doing the reverse acceleration movement (from BDC to TDC) in the time interval from 17.5 to 30 ms. In the time interval from 17.5 to 20 ms, due to the spring force, the electromagnetic force is not required, so the armature current is set still to be of zero. In the time interval from 20 to 30 ms, the armature current is set to be -20 A in order to obtain stable electromagnetic force. LEG is doing the reverse deceleration movement (from BDC to TDC) in the time interval from 30 to 37.5 ms, the armature current is set to be –20 A until the end of the compression stroke.

It is the power stroke from 37.5 to 50 ms. The spark plug ignites the fuel mixture at the beginning of the power stroke. The chemical energy of fuel is absorbed by LEG and the kickback device. The active controlling for the electromagnetic force and the output electric power of LEG to adjust the piston motion are obtained. During this period, the armature current that used to limit the velocity of the piston is set to be of –70 A in order to obtain large electromagnetic force.

It is the exhaust stroke from 50 to 80 ms. In the time interval from 50 to 55 ms, due to the spring force, the electromagnetic force is not required, so the armature current is set to be of zero. LEG does acceleration movement (from TDC to BDC) in the time interval from 55 to 66 ms and deceleration movement (from TDC to BDC) in the time interval from 66 to 80 ms, the armature current that used to limit the velocity of the piston is set to be of 25 A until the end of the exhaust stroke.

The electromagnetic force of LEG is shown in Fig. 18. It should be noted that the target current in all of the four strokes is set according to the required electromagnetic force of LEG.

The terminal voltage of UC banks (U_1) and the required terminal voltage of LEG $(U_{\rm AB})$ when LEG works in the electromotor mode during the intake stroke and the compression

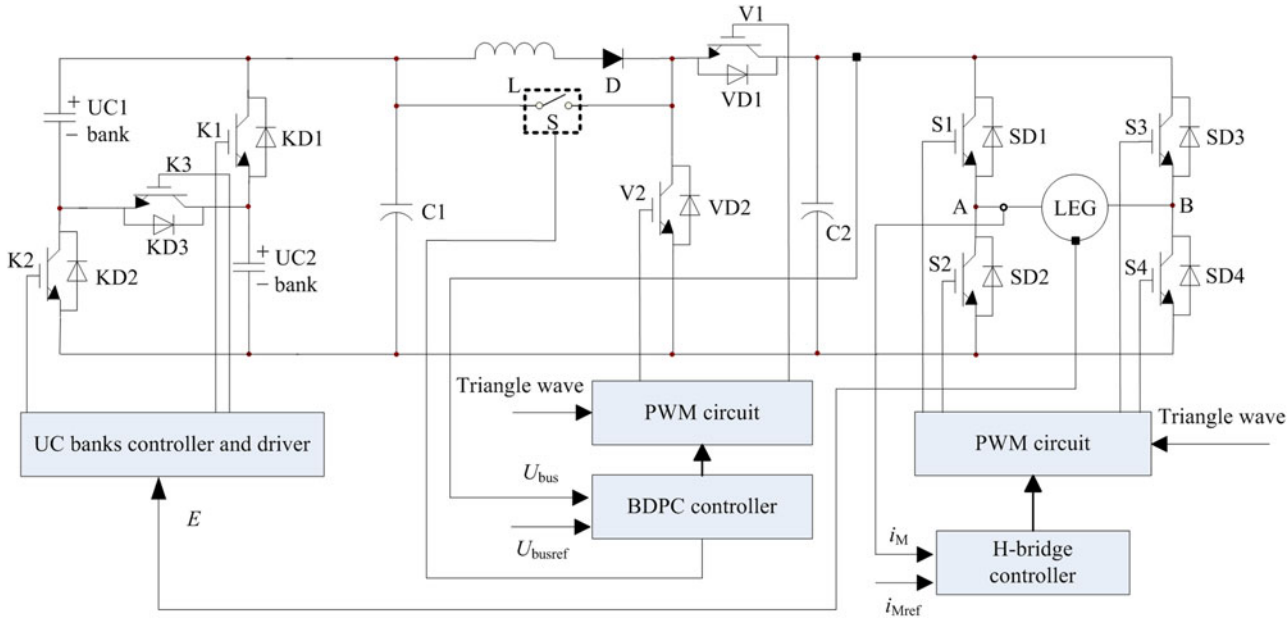

Fig. 16. Block diagram of the proposed novel energy storage system.

TABLE V
SPECIFICATION OF LEG

Items	Values
moving mass of piston assembly	3 [kg]
armature inductance	2.11 [mH]
interior resistance	0.14 [Ω]
maximal load force	4060 [N]
maximal armature current	100 [A]
electromagnetic force constant	40.6 [N/A]
back EMF constant	40.6 [V $(m/s)^{-1}$]
electromechanical time constant	0.31 [ms]

TABLE VI
SIMULATION PARAMETERS OF LEG

Items	Values
intake air pressure	1.4 [bar]
intake displacement	7∼45 [mm]
power displacement	7∼74 [mm]
reciprocating frequency	12.5 [Hz]
average output power	2.3 [kw]
generating efficiency	34% [−]

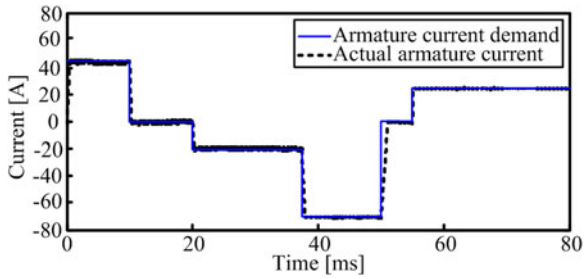

Fig. 17. Armature current tracking performance of LEG.

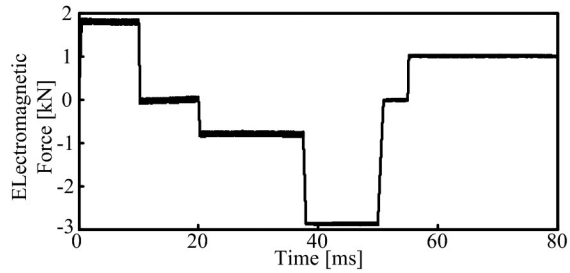

Fig. 18. Electromagnetic force of LEG.

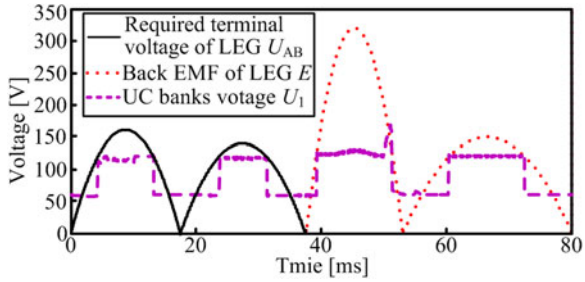

Fig. 19. Terminal voltage of UC banks, the required terminal voltage and the back EMF of LEG.

stroke are shown in Fig. 19. The required terminal voltage of LEG is mainly determined by velocity of the free piston during the intake stroke and the compression stroke. To illustrate the relationship between the required terminal voltage by LEG and the terminal voltage of the UC banks, the required terminal voltage of LEG in the compression stroke is changed to be positive in Fig. 19. It is proved that UC banks are discharged in parallel (at this time, $U_1 = 60$ V) when $U_{\rm AB} < 2U_C$ and UC banks are discharged in series (at this time, $U_1 = 120$ V) when $U_{\rm AB} > 2U_C$. It can be seen that the terminal voltage of UC

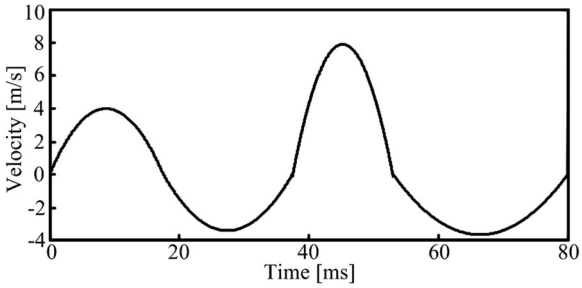

Fig. 20. Velocity of the free piston.

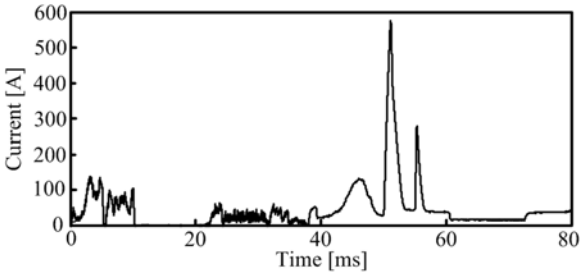

Fig. 21. Current of UC banks.

banks hardly decreases in the discharge process because of less energy released.

The terminal voltage of UC banks (U_1) and the back EMF of LEG (E) when LEG works in the generator mode during the power stroke and the exhaust stroke are also shown in Fig. 19. The back EMF of LEG is proportional to the velocity of the free piston during the power stroke and the exhaust stroke. To illustrate the relationship between the back EMF of LEG and the terminal voltage of the UC banks, the back EMF of LEG in the exhaust stroke is also changed to be positive in Fig. 19. The simulation curves show that UC banks are charged in parallel (at this time, $U_1 = 60\,\mathrm{V}$) when $E < 2U_C$ and UC banks are charged in series (at this time, $U_1 = 120\,\mathrm{V}$) when $E > 2U_C$, it also can be seen that the terminal voltage of UC banks hardly increases in the charging process because of less energy absorbed. The velocity of the free piston is shown in Fig. 20.

The current of UC banks is depicted in Fig. 21. It is the discharge current in motor operation where BDPC mainly works in boost operation. Therefore, the discharge current of UC banks is the pulsated current. It is the charge current in generator operation where BDPC mainly works in buck operation and transfers power to UC banks and charges the bus capacitor $C2$ at the same time. In the time interval from 50 to 55 ms, the required armature current is zero, so there is no power output, the stored energy of bus capacitor $C2$ is released to charge UC banks through BDPC.

The power requirement of LEG (P_M) and the power delivered to LEG (P_{UC}) in motor operation are shown in Fig. 22. The output power (P_M) of LEG and the absorbed power (P_{UC}) by UC banks in generator operation are also shown in Fig. 22.

Because of power conversion and transformation between power source and LEG, there are a part of power losses in the middle parts, such as parasitic parameters (inductances, capacitances, and resistances) of circuit and components. Losses generated by UC banks, LEG, switch components, and energy storage components are a significant part of the total lost power. Simulation results confirmed that efficiency of the ESS is 93.5%.

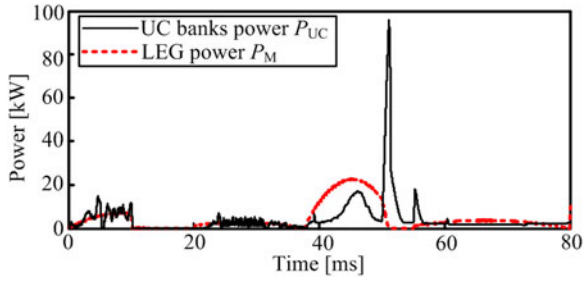

Fig. 22. Power of UC banks (P_{UC}) and power of LEG (P_{M}).

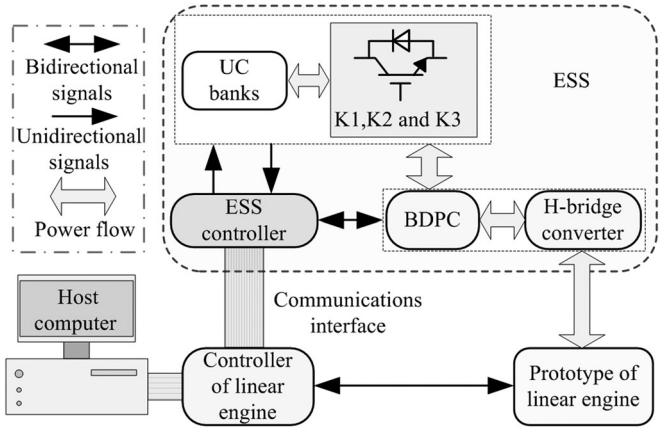

Fig. 23. Schematic diagram of the experimental system for ESS of linear engine.

The tuning of PID controller is a difficult problem, because it must satisfy complex criteria within the limitations of PID controller. In this paper, the traditional method is used to adjust the parameters of the PID controller, such as the proportional coefficient, the internal coefficient, and the derivative coefficient, it is required to do a lot of experiments repeatedly through computer simulations until the best responses of the transient and steady behavior of the closed-loop system are achieved. From the simulation results, we can conclude that the control system can efficiently track the demand, UC banks can be switched over between serial and parallel modes in real time, and the bus voltage is also effectively controlled.

IV. Experimental Results

To test the feasibility of the novel ESS and the power flow control strategy, an experimental system was set up. The controller is implemented by the TMS320F2812, which is a digital signal processor (DSP) possessing 150 MHz dominant frequency from Texas Instruments. Some experimental results based on working states are given in the following section.

Schematic diagram of the experimental system for ESS of linear engine is shown in Fig. 23. The experimental system mainly consists of three parts: the novel ESS, the physical prototype of linear engine and its controller, and the host computer. The local

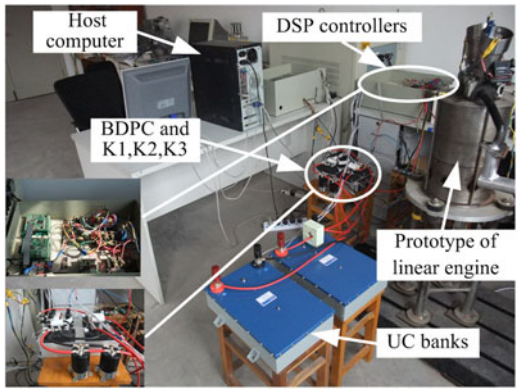

Fig. 24. Experimental platform for linear engine.

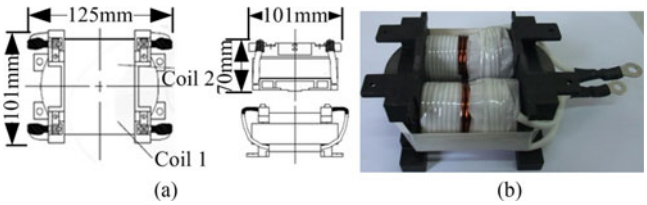

Fig. 25. Power inductor for BDPC. (a) Size of power inductor. (b) Structure of power inductor.

interconnect network is used to communicate and transfer data between controller of ESS and controller of linear engine. The data are sent to the host computer for analysis and processing.

The physical prototype of linear engine that has one cylinder is implemented by a DSP-based development platform in the laboratory, the experimental platform for linear engine is shown in Fig. 24, the main parameters of the physical prototype of linear engine are as follows: the moving mass of piston assembly is 3 kg, maximal load force of LEG is the 4100 N at the rated current of 100 A, the maximum stroke of LEG is 70 mm without thrust ripple, and the average output power is 2.2 kW.

The power switch devices (IGBTs) are used in UC banks with series-parallel connections switchover. The IGBTs of BDPC and H-bridge converter are 2MBI600U2E-060 (600 V/600 A) from Fuji Electric Device Technology, and a 15 kHz fixed-frequency PWM block is applied on IGBTs to control the power back and forth. The core material of the power inductor (125 μH/88 A) designed for BDPC is Fe-Al-Si, and the winding wire of the power inductor is 2.4 mm and the number of turns of it is 46. Meanwhile, the dc internal resistance of the power inductor is 8.9 mΩ. The size and structure of power inductor are shown in Fig. 25. The Hall effect based current sensors with wide dynamic range from –200 to 200 A and voltage sensors with wide dynamic range from –300 to 300 V are used in the experiment system.

The experiment research is performed based on the above experiment system. The piston motion of prototype during a four-stroke working cycle is measured. The target parameters of the piston motion as follows: BDC of the intake stroke is "$x_1^* = 50$ mm," TDC of the compression stroke is "$x_2^* = 10$ mm," BDC of the power stroke is "$x_3^* = 50$ mm," TDC of the exhaust stroke is "$x_4^* = 10$ mm." Some experimental results of the prototype with 10 bar cylinder pressure are shown in Fig. 26.

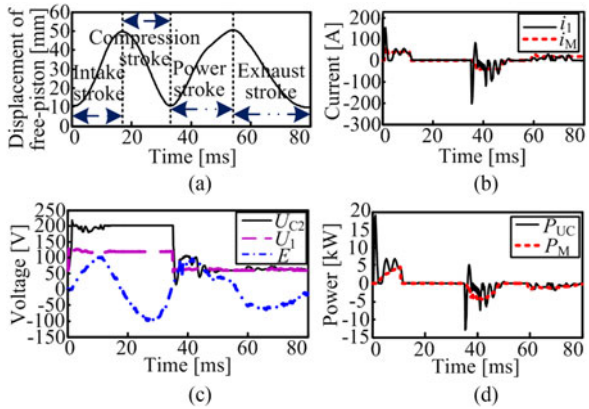

Fig. 26. Experimental waveforms of the prototype with 10 bar cylinder pressure. (a) Motion trajectory of the free piston. (b) LEG current and UC banks current. (c) Terminal voltage of UC banks, the back EMF of LEG and the high terminal voltage output of BDPC. (d) Instantaneous electric power.

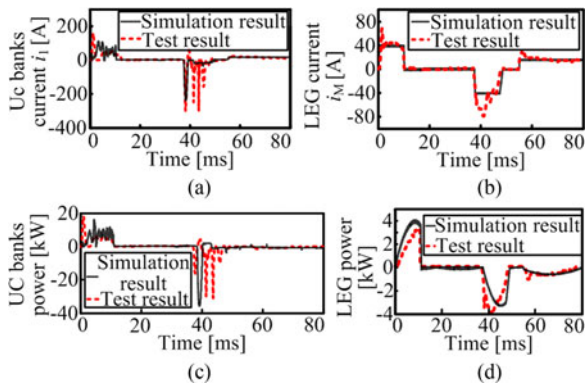

Fig. 27. Comparison between simulation results and experimental results of the prototype with 18 bar cylinder pressure. (a) UC banks current. (b) LEG current. (c) UC banks power. (d) LEG power.

The motion trajectory of the free piston is shown in Fig. 26(a). As is shown, the movement of the free piston can precisely reach the target. LEG current (i_M) and UC banks current (i_1) are shown in Fig. 26(b). The terminal voltage of UC banks (U_1), the back EMF of LEG (E) and the terminal voltage output of BDPC (U_{C2}) are shown in Fig. 26(c). In this experiment, UC banks are discharged in series (at this time, $U_1 = 120$ V) when LEG is working in motor operation. By the PID controller, BDPC is controlled to regulate the high output voltage at 200 V. As can be seen, the output voltage can reach the set voltage value at $t =$ 2 ms without sudden crease. The curves show that UC banks are charged in parallel (at this time, $U_1 = 60$ V) when $E < 120$ V in generator operation. Instantaneous electric power is shown in Fig. 26(d). The experiment results show that the efficiency of the four-stroke linear engine is nearly up to 34%, which is much higher than the conventional ICE. The efficiency of the designed novel ESS is up to 86.9%, meeting high efficiency requirements of the system.

In the case of the above-mentioned motion trajectory of the free piston of the prototype [as shown in Fig. 26(a)] with 10 bar cylinder pressure (one case study), a comparison between some simulation results and experimental results of the prototype with 18 bar cylinder pressure (the other case study) is shown in Fig. 27. As can be seen from the figure, the simulation

and experimental results are almost exactly matched. This can further show the validity of the ESS.

V. Conclusion

This paper systematically presents the researches on a dynamic model of a novel ESS, which mainly consists five parts: the UC banks which are switched over between serial and parallel with controller, an optimized BDPC with PID controller, H-bridge converter with PID controller, LEG of linear engine and power flow control strategy. In order to describe the dynamic behavior of the system, the mathematical models and Simulink models of the ESS are proposed. Based on these work, the overall Simulink model is presented, in which all sub-models of ESS are clearly identified. The waveforms of LEG armature current, UC banks terminal voltage, UC banks charge/discharge current, and the input and output characteristics of BDPC are also discussed and verified. Furthermore, an experimental system is established to test the feasibility of the novel ESS and the power flow control strategy. The design and control strategy of the novel ESS are proved to be efficient and accurate by simulation and experimental results.

References

[1] P. Kyle and S. H. Kim, "Long-term implications of alternative light-duty vehicle technologies for global greenhouse gas emissions and primary energy demands," *Energy Policy*, vol. 39, no. 5, pp. 3012–3024, 2011.

[2] F. Odeim, J. Roes, L. Wülbeck, and A. Heinzel, "Power management optimization of fuel cell/battery hybrid vehicles with experimental validation," *J. Power Sources*, vol. 252, pp. 333–343, 2014.

[3] J. Pinkse, R. Bohnsack, and A. Kolk, "The role of public and private protection in disruptive innovation: The automotive industry and the emergence of low—emission vehicles," *J. Prod. Innov. Manage.*, vol. 31, no. 1, pp. 43–60, 2014.

[4] B. Tang, X. Wu, and X. Zhang, "Modeling the CO_2 emissions and energy saved from new energy vehicles based on the logistic-curve," *Energy Policy*, vol. 57, pp. 30–35, 2013.

[5] F. M. Özel, C. S. Ernst, H. C. Davies, and L. Eckstein, "Development of a battery electric vehicle sector in North-West Europe: Challenges and strategies," *Int. J. Elect. Hybrid Veh.*, vol. 5, no. 1, pp. 1–14, 2013.

[6] H. Gong, M. Q. Wang, and H. Wang, "New energy vehicles in China: Policies, demonstration, and progress," *Mitigation Adapt. Strategies Global Change*, vol. 18, no. 2, pp. 207–228, 2013.

[7] Y. F. Wang, K. P. Li, X. M. Xu, and Y. R. Zhang, "Transport energy consumption and saving in China," *Renew. Sustain. Energy Rev.*, vol. 29, pp. 641–655, 2014.

[8] X. Yuan, X. Liu, and J. Zuo, "The development of new energy vehicles for a sustainable future: A review," *Renew. Sustain. Energy Rev.*, vol. 42, pp. 298–305, 2015.

[9] A. W. Bhutto, A. A. Bazmi, and G. Zahedi, "Greener energy: Issues and challenges for Pakistan—wind power prospective," *Renew. Sustain. Energy Rev.*, vol. 20, pp. 519–538, 2013.

[10] M. A. Hannan, F. A. Azidin, and A. Mohamed, "Hybrid electric vehicles and their challenges: A review," *Renew. Sustain. Energy Rev.*, vol. 29, pp. 135–150, 2014.

[11] B. Gu, C. Y. Lin, B. F. Chen, J. Dominic, and J. S. Lai, "Zero-voltage-switching PWM resonant full-bridge converter with minimized circulating losses and minimal voltage stresses of bridge rectifiers for electric vehicle battery chargers," *IEEE Trans. Power Electron.*, vol. 28, no. 10, pp. 4657–4667, Oct. 2013.

[12] N. B. Hung, O. Lim, and N. Iida, "The effects of key parameters on the transition from SI combustion to HCCI combustion in a two-stroke free piston linear engine," *Appl. Energy*, no. 137, pp. 385–401, 2015.

[13] B. Jia, G. Tian, H. Feng, and A. P. Roskilly, "An experimental investigation into the starting process of free-piston engine generator," *Appl. Energy*, vol. 157, pp. 798–804, 2015.

[14] H. Feng, Y. Song, Z. Zuo, J. Shang, Y. Wang, and T. Roskilly, "Stable operation and electricity generating characteristics of a single-cylinder free piston engine linear generator: Simulation and experiments," *Energies*, vol. 8, no. 2, pp. 765–785, 2015.

[15] S. Q. Chang and Z. P. Xu, "Internal combustion-linear generator integrated power system," China Patent 10019410.0, Jan. 22, 2007.

[16] S. Q. Chang and Z. P. Xu, "Conceptual design of internal combustion-linear generator integrated power system," *J. Nanjing Univ. Sci. Technol. (Natural Sci.)*, vol. 32, no. 4, pp. 449–452, 2008.

[17] G. Z. Ren, G. Q. Ma, and N. Cong, "Review of electrical energy storage system for vehicular applications," *Renew. Sustain. Energy Rev.*, vol. 41, pp. 225–236, 2015.

[18] G. Z. Ren and S. Q. Chang, "Energy storage system with bi-directional electric power flow and its control method," China Patent 201010508339.4, Oct. 15, 2013.

[19] G. Z. Ren and S. Q. Chang, "A high-efficiency regenerative braking for electric vehicles," *J. Power Syst. Technol.*, vol. 35, no. 1, pp. 164–169, 2011.

[20] M. Patterson, N. F. Macia, and A. M. Kannan, "Hybrid microgrid model based on solar photovoltaic battery fuel cell system for intermittent load applications," *IEEE Trans. Energy Convers.*, vol. 30, no. 1, pp. 359–366, Mar. 2015.

[21] A. Nahavandi, M. T. Hagh, M. B. B. Sharifian, and S. Danyali, "A non-isolated multiinput multioutput dc–dc boost converter for electric vehicle applications," *IEEE Trans. Power Electron.*, vol. 30, no. 4, pp. 1818–1835, Apr. 2015.

[22] G. Yang, P. Dubus, and D. Sadarnac, "Double-phase high-efficiency, wide load range high- voltage/low-voltage LLC DC/DC converter for electric/hybrid vehicles," *IEEE Trans. Power Electron.*, vol. 30, no. 4, pp. 1876–1886, Apr. 2015.

[23] S. Weearsinghe, D. J. Thrimawithana, and U. K. Madawala, "Modeling bidirectional contactless grid interfaces with a soft DC-link," *IEEE Trans. Power Electron.*, vol. 30, no. 7, pp. 3528–3541, Jul. 2015.

[24] B. Hredzak, V. G. Agelidis, and M. Jang, "A model predictive control system for a hybrid battery-ultracapacitor power source," *IEEE Trans. Power Electron.*, vol. 29, no. 3, pp. 1469–1479, Mar. 2014.

[25] D. B. Murray and J. G. Hayes, "Cycle testing of supercapacitors for long-life robust applications," *IEEE Trans. Power Electron.*, vol. 30, pp. 2505–2516, May 2015.

[26] 2016. [Online]. Available: http://cn.mathworks.com/help/physmod/sps/powersys/ref/supercapacitor.html

[27] E. Takahara, H. Sato, and J. Yamada, "Series and parallel connections change over system for electric double layer capacitors (EDLCs) to electric vehicle energy saving," in *Proc. Power Convers. Conf.*, 2002, pp. 577–581.

[28] G. Z. Ren and S. Q. Chang, "Optimization design of bi-directional DC/DC power converter of internal combustion-linear generator integrated power system," *J. Power Syst. Prot. Control*, vol. 39, no. 6, pp. 105–111, 2011.

[29] R. Zeng, L. Xu, L. Yao, and B. W. Williams, "Design and operation of a hybrid modular multilevel converter," *IEEE Trans. Power Electron.*, vol. 30, no. 3, pp. 1137–1146, Mar. 2015.

[30] Y. P. Hsieh, J. F. Chen, L. S. Yang, C. Y. Wu, and W. S. Liu, "High-conversion-ratio bidirectional dc–dc converter with coupled inductor," *IEEE Trans. Ind. Electron.*, vol. 61, no. 1, pp. 210–222, Jan. 2014.

[31] G. Z. Ren and S. Q. Chang, "A novel scheme design of UC banks based on series-parallel connections switchover for internal combustion-linear generator integrated power system," *Int. J. Elect. Hybrid Veh.*, vol. 3, no. 1, pp. 83–98, 2011.

[32] G. Z. Ren and S. Q. Chang, "Power flow control strategy of internal combustion-linear generator integrated power system," *J. Nanjing Univ. Sci. Technol.*, vol. 34, no. 6, pp. 781–786, 2010.

Guizhou Ren received the B.S. degree in computer science and technology and the M.S. degree in vehicle application engineering from the Shandong University of Technology, Zibo, China, in 2003 and 2007, respectively, and the Ph.D. degree in mechanical engineering from the Nanjing University of Science and Technology, Nanjing, China, in 2011.

From 2011 to 2015, he was a Lecturer with the Department of Vehicle Engineering, School of Electromechanical and Automotive Engineering, Yantai University, Yantai, China, and became an Associate Professor in December 2015.

His research interests include power supplies, energy conversion and storage, and AEVs.